Graphical Abstract

Radiation-Induced Negative Optical Nonlinearities in Fused Silica, Sapphire, and Borosilicate Glass

B. W. Morgan, M. P. Van Zile, C. M. Petrie, P. Sabharwall, M. Burger, I. Jovanovic

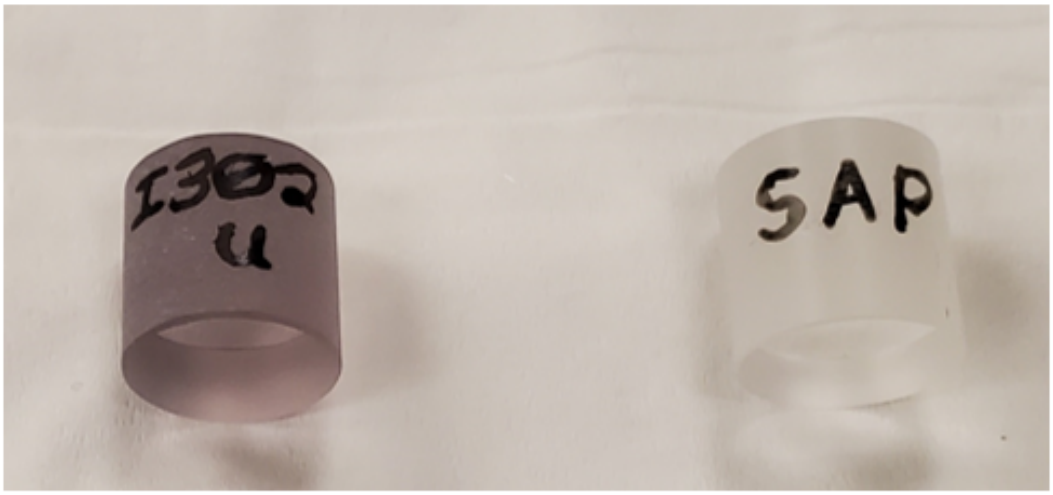

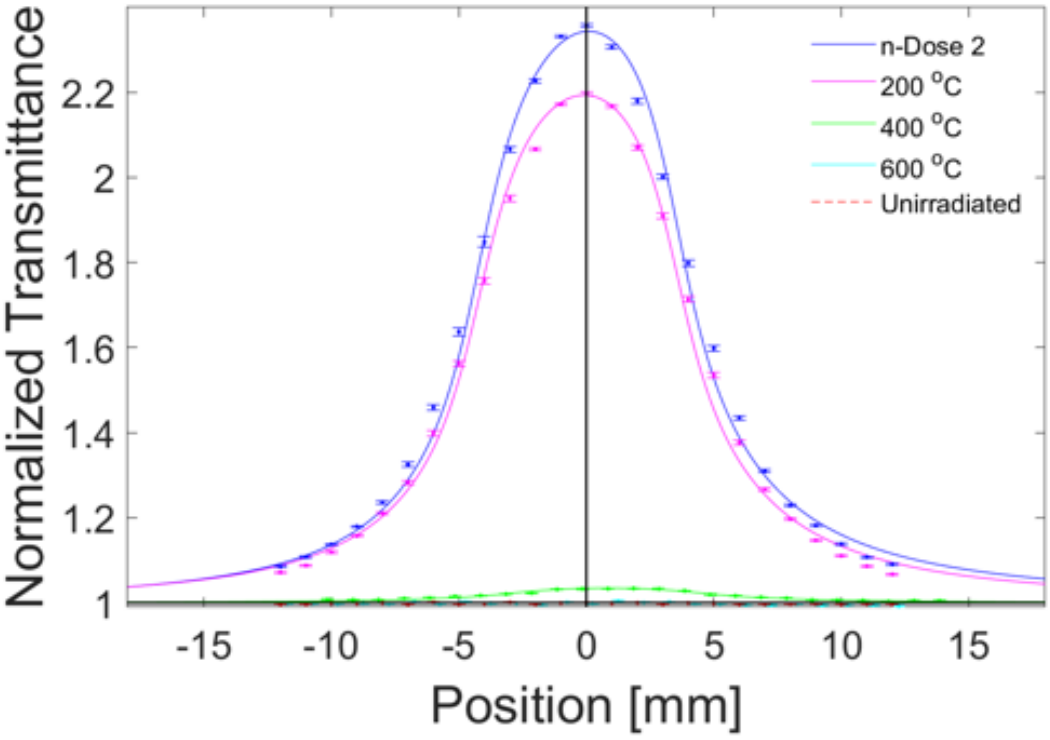

Highlights

Radiation-Induced Negative Optical Nonlinearities in Fused Silica, Sapphire, and Borosilicate Glass

B. W. Morgan, M. P. Van Zile, C. M. Petrie, P. Sabharwall, M. Burger, I. Jovanovic

- Radiation-induced negative nonlinear absorption is reported for the first time in fused silica, sapphire, and borosilicate glass
- Post-irradiation thermal annealing of optical materials is shown to anneal the negative nonlinear optical effects
- The effects of concurrent-irradiation thermal annealing are compared to post-irradiation thermal annealing to examine the competing rates of radiation damage and thermal annealing in optical materials
- A radiation-induced negative nonlinear refractive index is observed in radiation-resistant borosilicate glass

Radiation-Induced Negative Optical Nonlinearities in Fused Silica, Sapphire, and Borosilicate Glass

B. W. Morgan[a], M. P. Van Zile[c], C. M. Petrie[d], P. Sabharwall[e,1], M. Burger[a,1], I. Jovanovic[a,1]

[a]*Department of Nuclear Engineering and Radiological Sciences, The University of Michigan, 2355 Bonisteel Boulevard, Ann Arbor, 48109, Michigan, United States*
[b]*Center for Ultrafast Optical Science, 2200 Bonisteel Boulevard, Ann Arbor, 48109, Michigan, United States*
[c]*Nuclear Reactor Laboratory, The Ohio State University, 1298 Kinnear Road, Columbus, 43212, Ohio, United States*
[d]*Oak Ridge National Laboratory, 5200, 1 Bethel Valley Road, Oak Ridge, 37830, Tennessee, United States*
[e]*Idaho National Laboratory, 1955 North Fremont Avenue, Idaho Falls, 83415, Idaho, United States*

Abstract

Negative nonlinear absorption is reported in neutron- and gamma-irradiated high-OH content fused silica, low-OH content fused silica, sapphire, borosilicate glass, and radiation-resistant borosilicate glass irradiated to total neutron fluences of 3.4×10^{16} n $\cdot$ cm^{-2} (42 Mrad γ), 1.7×10^{17} n $\cdot$ cm^{-2} (211 Mrad γ), and 3.6×10^{17} n $\cdot$ cm^{-2} (433 Mrad γ). Nonlinear absorption coefficients were measured via Z-scan and are on the order of $-(10^{-14} - 10^{-10})$ m$\cdot$W^{-1}. The Z-scan also reveals a negative nonlinear index of refraction in neutron- and gamma-irradiated radiation-resistant borosilicate glass on the order of -10^{-19} m$^2\cdot$W^{-1}. Thermal annealing at temperatures up to 800 °C is shown to restore these nonlinearities to their positive unirradiated values in all four materials. All Z-scan measurements were performed at 532 nm with a nanosecond pulsed laser. The occurrence of negative nonlinearities may be attributed to the presence of metallic impurities and the resulting saturable absorption. A limited effect of photobleaching is observed in measurements and is quantified in multiple Z-scans.

Keywords: Nonlinear absorption, Z-scan, Radiation effects, optical materials
PACS: 0000, 1111
2000 MSC: 0000, 1111

1. Introduction

The performance of optical materials in extreme radiation and thermal environments is of great importance for advanced fission and fusion reactor systems [1, 2], accelerators [3], and space applications [4]. A fraction of these applications require the use of optics in laser-based optical instrumentation. Laser-induced breakdown spectroscopy (LIBS), which relies upon the application of high-power laser pulses and spectroscopic analysis, has realized broad applications across industries that include undersea and outer space exploration [5]. The development of LIBS-based optical sensors for the nuclear fission power generation industry and for spent nuclear fuel analysis has the potential to significantly enhance the safety and

economic efficiency of nuclear reactors through the provision of online and *in-situ* monitoring of internal reactor conditions [6, 1]. Real-time monitoring of fission reactor operating conditions, such as through analyzing off-gas stream of a molten salt reactor, has the potential to provide instantaneous information about the integrity of internal components of reactors, which could enhance safety and reduce the frequency of shutdowns for inspection [7, 8]. For the fusion reactors under development, LIBS has been considered as a method to measure impurities, and anti-corrosion materials, and to diagnose fuel retention in plasma-facing components [9, 10]. To accomplish these goals for instrumentation, a thorough understanding is needed of the radiation and thermal effects on various optical materials.

Fused silica, sapphire, and borosilicate glass are common and well-characterized materials used in many optical components, including windows and lenses. These materials and their variants, such as high-OH and low-OH content fused silica and radiation-resistant borosilicate glass, have a relatively well-understood linear index of refraction and linear absorption coefficient. These properties, along with the mechanical characteristics, damage threshold, and cost govern the selection of materials for various applications [11, 12]. The linear optical properties of materials have been found to change when exposed to ionizing radiation, thermal annealing, or a combination of the two, and these changes have also been extensively studied [13, 14, 15, 16, 17, 18, 19, 20, 2, 21, 22, 23, 24, 25, 26, 27, 28, 29, 30, 31].

The *nonlinear* optical properties of materials have a similarly significant impact on applications that require high-power laser pulse propagation, and have been studied and characterized since the advent of the laser [32, 11, 33]. However, the ionizing radiation-induced changes of the nonlinear optical properties have not seen a similar level of attention to date. Macroscopic nonlinear optical properties of materials depend on the light intensity and manifest as nonlinear refraction (NLR) and nonlinear absorption (NLA). They are usually parameterized as

$$n = n_0 + n_2 I, \tag{1}$$

$$\alpha = \alpha_0 + \beta I. \tag{2}$$

Here, n is the index of refraction, n_0 is the linear index of refraction, n_2 is the nonlinear index of refraction, α is the absorption coefficient, α_0 is the linear absorption coefficient, β is the NLA coefficient, and I is the light intensity. The NLR index and NLA coefficient represent the aggregate effects of multiple components of the third-order nonlinear susceptibility that contribute to nonlinear optical phenomena such as two-photon absorption (TPA), multiphoton absorption, saturable absorption (SA), reverse saturable absorption, excited-state absorption, electrostriction, and thermal effects [34, 35, 36]. The NLR and NLA coefficients can be measured by the technique referred to as Z-scan [32, 34, 37], which simultaneously captures all constituent effects. A Z-scan that employs a longer pulse duration (in the nanosecond range) is sensitive both to susceptibilities with fast and with slow excited state decay times so that the determination of the individual underlying physical processes from Z-scan alone is generally not possible [34]. Nonetheless, there are examples in the literature that describe Z-scan measurements of negative NLA coefficients and propose a competition between TPA, which results from an ultrafast nonlinear susceptibility, and SA, which represents a slow nonlinearity, that can lead to phenomena such as negative NLA in semiconductors, nanocomposites, thin films, and doped glasses [11, 38, 39, 40, 36, 41, 42].

Negative NLA has not been observed in bulk optical materials until the recent report of the gamma-radiation-induced negative nonlinear absorption in optical quartz glass [43]. Here we report that negative NLA following exposure to ionizing radiation is a more widespread phenomenon that takes place in multiple materials (Heraeus Spectrosil 2000 high-OH content and Infrasil 302 low-OH content fused silica, sapphire, Schott borosilicate glass, and Schott radiation-resistant borosilicate glass), that it occurs in response to both gamma and neutron irradiation, and that in addition to negative NLA, the irradiation can also induce a negative NLR. We further observe that the negative nonlinearities can be effectively thermally annealed in all materials studied, which is akin to the traditional restoration of linear optical transparency by thermal annealing.

2. Experiment

We constructed a post-irradiation examination (PIE) setup that incorporates the Z-scan technique to measure the changes in NLA and NLR following irradiation and thermal annealing. The setup is mobile and self-contained such that it can be readily deployed at the site of irradiation, alleviating the concerns with the transport of potentially activated materials and significant measurement delays after irradiation. The setup is described in detail in previous work [44, 43]. Briefly, the Z-scan measurement is performed with the second harmonic of a nanosecond Nd:YAG laser (532 nm), which is a common LIBS drive laser wavelength. The Z-scans were performed in the thick-sample regime, where the sample thickness, L, is greater than the Rayleigh length of the laser beam at focus, z_R, such that the Z-scan signal can be enhanced [34]. The first-order theory of Hermann and McDuff for weak nonlinearities is used to model the results of the Z-scan and extract the NLA and NLR coefficients [45]. Z-scan measurements were performed for all samples prior to and after irradiation. Some samples were measured after irradiation with concurrent-irradiation thermal annealing. Others were measured after irradiation and subsequent post-irradiation thermal annealing steps.

Table 1: Optical sample information

Material	Vendor	Type	OH Content
High-OH Fused Silica	Heraeus	Spectrosil 2000	$\leq$ 1300 ppm
Low-OH Fused Silica	Heraeus	Infrasil 302	$\leq$ 8 ppm
Sapphire	Guild Optical Associates	Optical Grade	
Borosilicate Glass	Schott JML Optical	NBK7	
Borosilicate Glass	Schott JML Optical	BK7G18	

The samples examined are listed in Table 1. All samples were cylinders with a thickness of 12.7 mm and a diameter of 12.7 mm, and the Z-scan laser axis of propagation (z-axis)

was parallel to the axis of the cylinder. Spectrosil 2000 (S2000) fused silica is a type III commercial silica with a high purity and high-OH content [12]. Infrasil 302 (I302) fused silica is a type I commercial silica with a higher metallic impurity content than type III, the most significant being aluminum (20 ppm), and a lower OH content [12]. The sapphire samples were of optical grade with the c-axis normal to the flat optical face. The Schott borosilicate glass (NBK7) is a popular and common crown glass free of lead and arsenic with high transmission range down to 350 nm, and the Schott radiation-resistant borosilicate glass (BK7G18) is crown glass doped with 1.8 w% cerium. The samples are shown in Figure 1 after irradiation to a total neutron fluence of 3.4×10^{16} n $\cdot$ cm^{-2} (42 Mrad γ). Prior to irradiation, the apparent transparency of all samples was similar to that of Spectrosil 2000, which is shown on the left side in Figure 1(a).

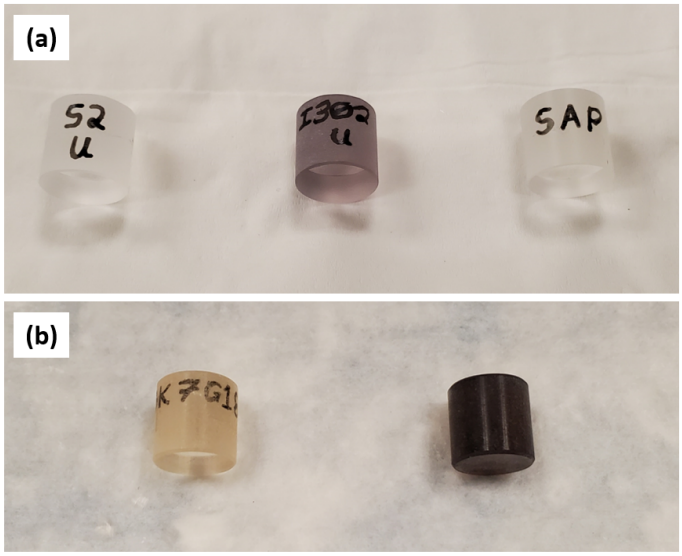

Figure 1: Window samples after irradiation to a total neutron fluence of 3.4×10^{16} n $\cdot$ cm^{-2} (42 Mrad γ). (a) From left to right: Spectrosil 2000, Infrasil 302, and sapphire. (b) Left: BK7G18 and right: NBK7.

Irradiations and thermal annealing were performed at The Ohio State University Nuclear Reactor Laboratory. The samples were irradiated in the air while being suspended within custom-fabricated thermal annealing furnaces that were inserted into the 6.5-inch diameter dry tube adjacent to the nuclear reactor core. All irradiations were performed in this manner, including those where concurrent and post-irradiation thermal annealing were studied, to ensure the consistency of sample radiation exposure for comparison. The total neutron flux was measured within the furnace by irradiating bare and cadmium-covered sets of flux wires with different thermal and resonant absorption peaks, and then integrating the kerma factor as a function of energy over the range of the neutron flux spectrum [28, 46]. The total neutron flux was 1.7×10^{12} n $\cdot$ cm^{-2}s^{-1}, with a thermal flux of 1.3×10^{12} n $\cdot$ cm^{-2}s^{-1}, fast (epi-cadmium, $E_n > 0.5$ eV) flux of 4.4×10^{11} n $\cdot$ cm^{-2}s^{-1}, and gamma dose rate of 7.6×10^{6} rad $\cdot$ hr^{-1}.

Thermal annealing was performed either post-irradiation or concurrently with irradiation, using equivalent neutron fluences in both cases. The irradiation of samples with post-irradiation thermal annealing was conducted to evaluate the radiation-induced alterations in

the optical materials, and then to determine the efficacy of thermal annealing in restoring the sample properties to the unirradiated state. Equivalent sample irradiations were performed again with concurrent-irradiation thermal annealing to evaluate the efficacy of thermal annealing while the samples are being irradiated, and to determine if the thermal annealing can repair radiation damage at a rate greater than the rate at which damage is generated. Post-irradiation thermal annealing was performed at 200 °C, 400 °C, 600 °C, and 800 °C, with the samples annealed at each temperature for 30 minutes. The NBK7 and BK7G18 samples were annealed only to 400 °C because of their melting points. Concurrent-irradiation thermal annealing was performed by heating the samples to 800 °C for the duration of the irradiation using the custom-fabricated furnaces within the nuclear reactor dry tube. Again, the NBK7 and BK7G18 samples were excluded from the concurrent-irradiation thermal annealing experiments due to their lower melting points. Table 2 summarizes the test conditions and identifies three characteristic neutron fluences (referred to as n-Dose 1, n-Dose 2, and n-Dose 3) and the associated gamma doses.

Table 2: Irradiation and thermal annealing conditions. The estimated gamma dose for each neutron fluence is provided in parentheses. All neutron fluences are total (fast and thermal).

Label	Fluence/Dose	Anneal Type	Temp.	Time
n-Dose 1	3.4×10^{16} n · cm^{-2} (42 Mrad)	Post	200 °C 400 °C 600 °C 800 °C	30 min. 30 min. 30 min. 30 min.
n-Dose 1	3.4×10^{16} n · cm^{-2} (42 Mrad)	Concurrent	800 °C	Duration
n-Dose 2	1.7×10^{17} n · cm^{-2} (211 Mrad)	Post	200 °C 400 °C 600 °C 800 °C	30 min. 30 min. 30 min. 30 min.
n-Dose 2	1.7×10^{17} n · cm^{-2} (211 Mrad)	Concurrent	800 °C	Duration
n-Dose 3	3.6×10^{17} n · cm^{-2} (443 Mrad)	Not Annealed		
n-Dose 3	3.6×10^{17} n · cm^{-2} (443 Mrad)	Concurrent	800 °C	Duration

3. Results

Figures 2, 3, and 4 show the results of NLA measurements for S2000, I302, and sapphire, respectively, for three irradiation doses and with post- and concurrent-irradiation thermal annealing. In all plots, the unirradiated Z-scan measurement is included for comparison. The point within each sample where the maximum nonlinear effect occurs is indicated on each Z-scan plot at $Z = 0$. The location of the maximum nonlinear effect varies based on the

Rayleigh length of the Z-scan, the sample thickness, the beam quality, and the strength of the material's nonlinear properties [45]. For the conditions of this experiment, $Z = 0$ occurs within the sample after the sample midpoint in the direction of laser propagation. The standard error evaluated for 40 measurements at each position is included in all Z-scan plots. All three samples annealed to the unirradiated state after heating to 400 °C for 30 minutes except I302, which after n-Dose 2 required heating to 600 °C. Annealing at 400 °C had the most significant effect in restoring all three materials' optical properties to the unirradiated state. Annealing at 200 °C reduced the negative nonlinearity by a fraction but did not restore it to the unirradiated state. The opposite of this trend is observed later in the borosilicate glass samples. Finally, concurrent-irradiation thermal annealing at 800 °C maintained S2000 and sapphire at the unirradiated NLA state within the measurement uncertainty, but I302 accumulated radiation effects during concurrent-thermal annealing resulting in a negative NLA coefficient, evident in Figures 3(d), 3(e), and 3(f).

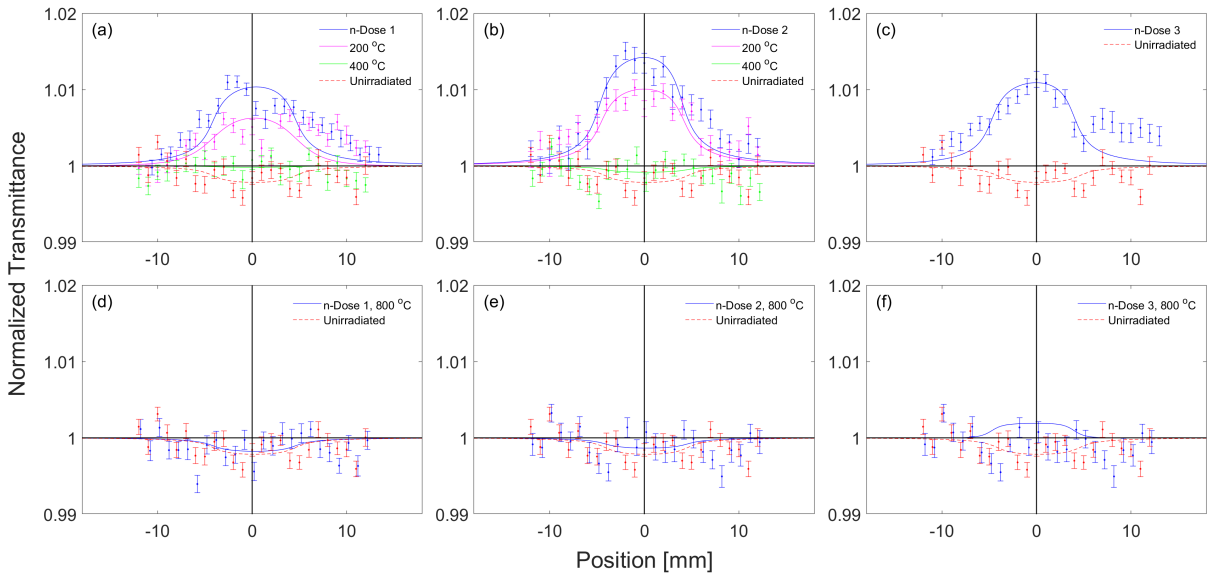

Figure 2: NLA measurements of Spectrosil 2000 after (a) irradiation to n-Dose 1 and post-irradiation thermal annealing through 400 °C, (b) irradiation to n-Dose 2 and post-irradiation thermal annealing through 400 °C, (c) irradiation to n-Dose 3, (d) irradiation to n-Dose 1 with concurrent-irradiation thermal annealing at 800 °C, (e) irradiation to n-Dose 2 with concurrent-irradiation thermal annealing at 800 °C, and (f) irradiation to n-Dose 3 with concurrent-irradiation thermal annealing at 800 °C.

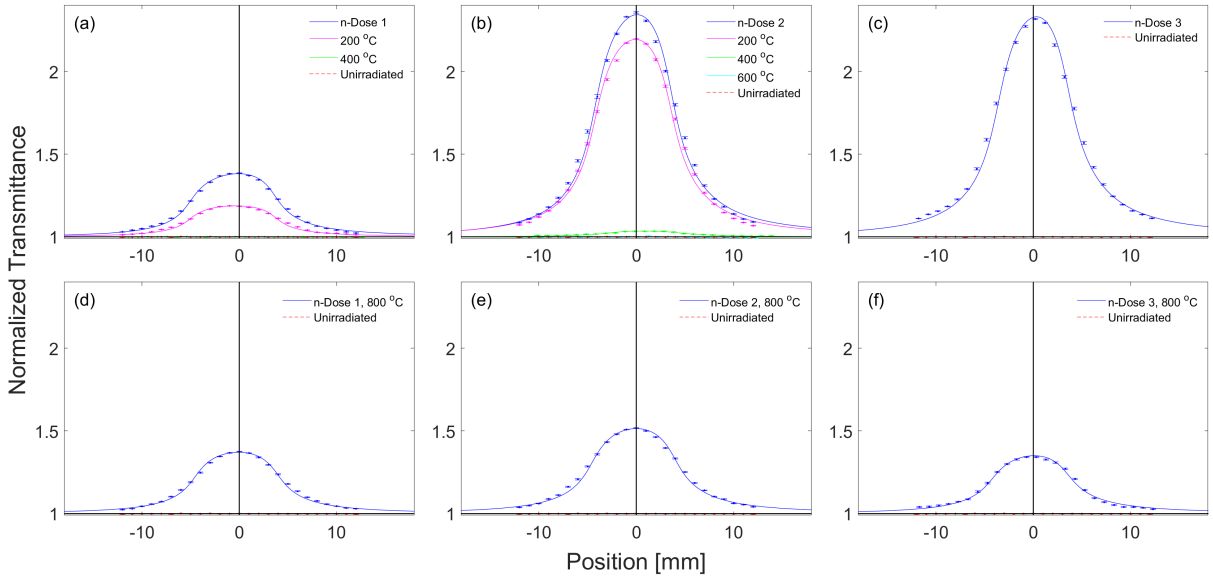

Figure 3: NLA measurements of Infrasil 302 after (a) irradiation to n-Dose 1 and post-irradiation thermal annealing through 400 °C, (b) irradiation to n-Dose 2 and post-irradiation thermal annealing through 400 °C, (c) irradiation to n-Dose 3, (d) irradiation to n-Dose 1 with concurrent-irradiation thermal annealing at 800 °C, (e) irradiation to n-Dose 2 with concurrent-irradiation thermal annealing at 800 °C, and (f) irradiation to n-Dose 3 with concurrent-irradiation thermal annealing at 800 °C.

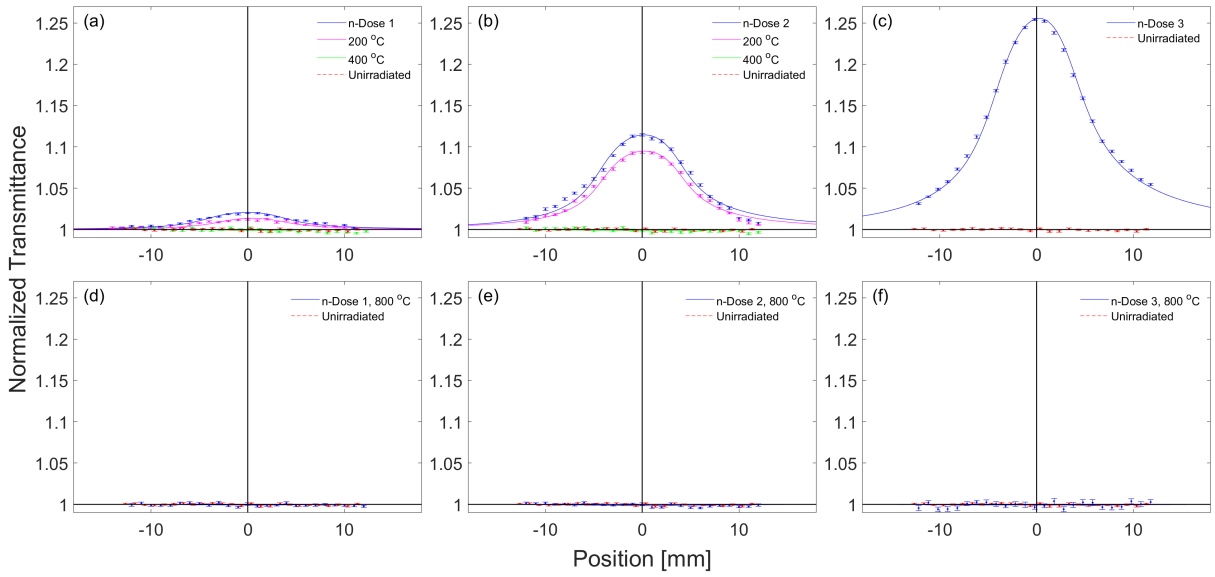

Figure 4: NLA measurements of sapphire after (a) irradiation to n-Dose 1 and post-irradiation thermal annealing through 400 °C, (b) irradiation to n-Dose 2 and post-irradiation thermal annealing through 400 °C, (c) irradiation to n-Dose 3, (d) irradiation to n-Dose 1 with concurrent-irradiation thermal annealing at 800 °C, (e) irradiation to n-Dose 2 with concurrent-irradiation thermal annealing at 800 °C, and (f) irradiation to n-Dose 3 with concurrent-irradiation thermal annealing at 800 °C.

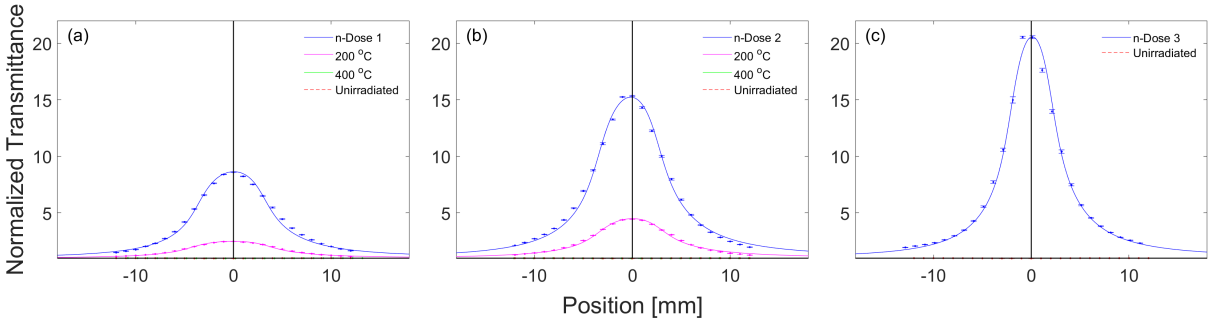

Figure 5: NLA measurements of NBK7 after (a) irradiation to n-Dose 1 and post-irradiation thermal annealing through 400 °C, (b) irradiation to n-Dose 2 and post-irradiation thermal annealing through 400 °C, and (c) irradiation to n-Dose 3.

Figure 5 shows the results of post-irradiation thermally annealed NLA measurements for NBK7 glass. NBK7 exhibited the greatest magnitude of negative NLA, which appears correlated with the high opacity of NBK7 after irradiation, as seen in Figure 1(b). The majority of thermal annealing occurs when heating the sample to 200 °C, and the sample fully anneals at 400 °C. BK7G18 similarly exhibited a negative NLA coefficient that annealed after heating to 400 °C, shown in Figures 6(a), 6(b), and 6(c). BK7G18 also exhibited a negative NLR index that had a consistent and expected form, shown in Figures 6(d) and 6(e) with fit lines. The unirradiated and 400 °C annealed NLR curves were not discernible, possibly due to darkening that has been observed during Z-scans in some BK7 samples [37]. The irradiated curves, however, were highly symmetric and consistent, and an NLR index was extracted from these. It is also observed that after annealing to 400 °C the NLR curves show more significant decreases in transmission than the unirradiated curves, which can be attributed to the previously noted darkening enhanced by irradiation.

NBK7, and to a lesser degree BK7G18, sapphire, and I302, exhibited an effect that resembles photobleaching. This was apparent when performing multiple Z-scans on the same spot of an irradiated sample and obtaining increasing transmission peak magnitudes in each subsequent Z-scan. This effect was tested in NBK7 irradiated to n-Dose 2 and is shown in Figure 7. During this test, the irradiated NBK7 sample was moved to the position of maximum transmission (0 mm), and the laser was pulsed continuously at the same sample location. Measurements of the open aperture and reference photodiodes were taken at periodic time intervals over 3 hours; the ratio of the open aperture diode (which measures the transmitted power) to reference diode (which measures the incident power) with a power fit is plotted in Figure 7. It can be seen that over time the rate of photobleaching decreases. Potential photobleaching was also observed through consecutive Z-scans performed on the same location in the material for irradiated I302, sapphire, NBK7, and BK7G18, which is presented in Figs. A.9, A.10, A.11, and A.12 in the Appendix.

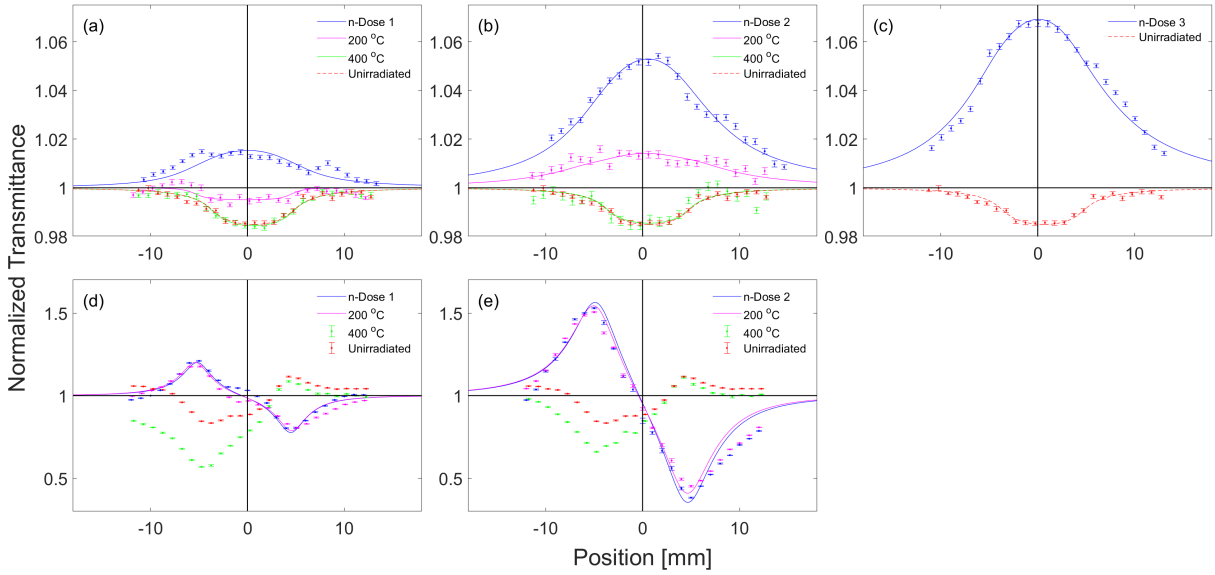

Figure 6: NLA measurements of BK7G18 after irradiation to (a) n-Dose 1 and (b) n-Dose 2, both with post-irradiation thermal annealing through 400 °C, (c) after irradiation to n-Dose 3, and the corresponding NLR measurements of BK7G18 after irradiation to (c) n-Dose 1 and (d) Dose 2, both with post-irradiation thermal annealing through 400 °C. Z-scans in (d) and (e) without a fit line were unable to be reliably simulated.

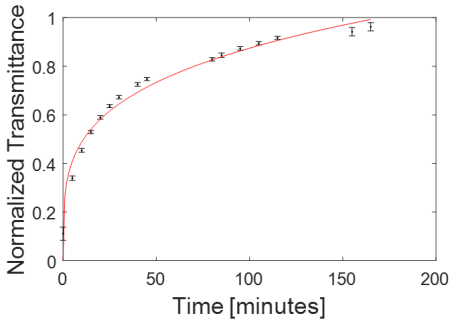

Figure 7: Photobleaching test of NBK7 sample irradiated to n-Dose 2. The sample is moved to the position of maximum transmitted intensity (0 mm), and the laser is pulsed continuously at a repetition rate of 10 Hz. At each time interval identified in the plot 120 pulses are recorded, and the ratio of power transmitted to the open aperture photodiode and to the reference photodiode is plotted with a power fit (red).

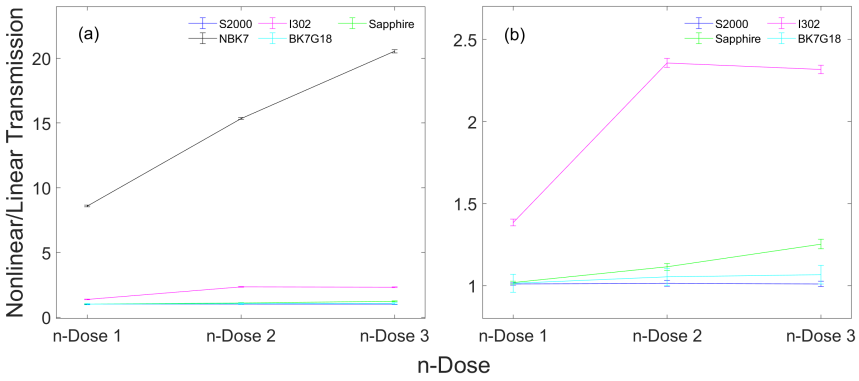

Figure 8: Comparison of the 532 nm radiation induced nonlinear transmission and linear transmission after n-Dose 1, 2, and 3 for (a) S2000, I302, Sapphire, NBK7, and BK7G18, and (b) at a reduced scale for S2000, I302, sapphire, and BK7G18.

Table 3 lists the NLA and NLR coefficients extracted from the fit to measured Z-scan curves in irradiated and thermally annealed samples. The unirradiated NLA coefficients are obtained from literature and are used to calibrate the Z-scan using an NBK7 sample [11, 43]. All of the values presented correspond to the Z-scan fits provided in the figures in the Results section. Irradiated n_2 values are omitted for all samples, except for BK7G18, because the irradiated closed aperture Z-scans were inconsistent, and the nonlinear index of refraction was not able to be determined by fitting to a simulated Z-scan. Attempts were made to determine n_2 by taking the ratio of powers measured with the closed aperture and the open aperture measurement to obtain an accurate NLR estimate in the presence of NLA but were not successful [34]. Concurrent-irradiation thermal annealing NLA coefficient values for borosilicate glass samples are omitted because, as mentioned in the Experiment section, the melting point of borosilicate glass precluded it from being thermally annealed to 800 °C. Finally, only I302 has an NLA coefficient listed for n-Dose 2 thermally annealed to 600 °C because all of the other samples annealed to the unirradiated state at 400 °C.

Table 3: Z-scan measured nonlinear coefficient. The provided unirradiated values are from literature [11].

Nonlinearity	n-Dose Anneal Temp.	Optical Sample				
		S2000	I302	Sapphire	NBK7	BK7G18
β [m·W^{-1}]	Unirradiated	$(< 5) \times 10^{-15}$	$(< 5) \times 10^{-15}$	$(< 1.6) \times 10^{-14}$	$(2.8) \times 10^{-14}$	$(2.8) \times 10^{-14}$
β [m·W^{-1}] Post-irradiation Annealing	n-Dose 1	$(-1.96 \pm 0.31) \times 10^{-14}$	$(-1.21 \pm 0.01) \times 10^{-12}$	$(-4.04 \pm 0.20) \times 10^{-14}$	$(-1.01 \pm 0.02) \times 10^{-11}$	$(-1.86 \pm 0.27) \times 10^{-14}$
	n-Dose 1 200 °C	$(-7.01 \pm 1.20) \times 10^{-15}$	$(-7.61 \pm 0.07) \times 10^{-13}$	$(-2.37 \pm 0.21) \times 10^{-14}$	$(-1.67 \pm 0.05) \times 10^{-12}$	$(1.53 \pm 0.32) \times 10^{-14}$
	n-Dose 1 400 °C	$(2.50 \pm 2.31) \times 10^{-15}$	$(5.16 \pm 4.40) \times 10^{-15}$	$(2.50 \pm 3.86) \times 10^{-15}$	$(2.91 \pm 0.30) \times 10^{-14}$	$(2.86 \pm 0.25) \times 10^{-14}$
	n-Dose 2	$(-2.33 \pm 0.32) \times 10^{-14}$	$(-5.01 \pm 0.02) \times 10^{-12}$	$(-1.74 \pm 0.04) \times 10^{-13}$	$(-1.99 \pm 0.05) \times 10^{-11}$	$(-5.77 \pm 0.27) \times 10^{-14}$
	n-Dose 2 200 °C	$(-1.55 \pm 0.21) \times 10^{-14}$	$(-4.48 \pm 0.02) \times 10^{-12}$	$(-1.47 \pm 0.04) \times 10^{-13}$	$(-4.41 \pm 0.02) \times 10^{-12}$	$(-1.23 \pm 0.24) \times 10^{-14}$
	n-Dose 2 400 °C	$(1.20 \pm 2.50) \times 10^{-15}$	$(-9.17 \pm 0.55) \times 10^{-14}$	$(1.99 \pm 2.62) \times 10^{-15}$	$(2.84 \pm 0.31) \times 10^{-14}$	$(2.66 \pm 0.51) \times 10^{-14}$
	n-Dose 2 600 °C	-	$(2.85 \pm 6.33) \times 10^{-15}$	-	-	-
	n-Dose 3	$(-1.85 \pm 0.30) \times 10^{-14}$	$(-4.90 \pm 0.02) \times 10^{-12}$	$(-3.66 \pm 0.03) \times 10^{-13}$	$(-3.71 \pm 0.02) \times 10^{-11}$	$(-7.68 \pm 0.24) \times 10^{-14}$
β [m·W^{-1}] Concurrent-irradiation Annealing	n-Dose 1 800 °C	$(2.66 \pm 3.41) \times 10^{-15}$	$(-1.27 \pm 0.02) \times 10^{-12}$	$(1.15 \pm 1.85) \times 10^{-15}$	-	-
	n-Dose 2 800 °C	$(2.03 \pm 3.21) \times 10^{-15}$	$(-1.98 \pm 0.01) \times 10^{-12}$	$(2.25 \pm 2.54) \times 10^{-15}$	-	-
	n-Dose 3 800 °C	$(-4.50 \pm 6.32) \times 10^{-15}$	$(-1.37 \pm 0.02) \times 10^{-12}$	$(0.55 \pm 6.54) \times 10^{-15}$	-	-
n_2 [m^2·W^{-1}] Post-irradiation Annealing	n-Dose 1	-	-	-	-	$(-1.70 \pm 0.04) \times 10^{-19}$
	n-Dose 1 200 °C	-	-	-	-	$(-1.67 \pm 0.03) \times 10^{-19}$
	n-Dose 2	-	-	-	-	$(-3.13 \pm 0.02) \times 10^{-19}$
	n-Dose 2 200 °C	-	-	-	-	$(-2.91 \pm 0.02) \times 10^{-19}$

Table 4: Z-scan post-irradiation measured nonlinear coefficient for three consecutive Z-scans to account for the photobleaching effect.

n-Dose Scan #	β [m·W^{-1}]				n_2 [m^2·W^{-1}]
	I302	Sapphire	NBK7	BK7G18	BK7G18
n-Dose 1 Scan 1	$(-8.27 \pm 0.01) \times 10^{-13}$	$(-3.20 \pm 0.25) \times 10^{-14}$	$(-9.26 \pm 0.04) \times 10^{-12}$	$(-2.58 \pm 0.29) \times 10^{-14}$	-
n-Dose 1 Scan 2	$(-1.05 \pm 0.01) \times 10^{-12}$	$(-3.52 \pm 0.20) \times 10^{-14}$	$(-1.00 \pm 0.03) \times 10^{-11}$	$(-2.44 \pm 0.30) \times 10^{-14}$	$(-1.08 \pm 0.03) \times 10^{-19}$
n-Dose 1 Scan 3	$(-1.21 \pm 0.01) \times 10^{-12}$	$(-4.04 \pm 0.20) \times 10^{-14}$	$(-1.01 \pm 0.02) \times 10^{-11}$	$(-1.86 \pm 0.27) \times 10^{-14}$	$(-1.70 \pm 0.04) \times 10^{-19}$
n-Dose 2 Scan 1	$(-4.35 \pm 0.02) \times 10^{-12}$	$(-1.58 \pm 0.03) \times 10^{-13}$	$(-1.94 \pm 0.01) \times 10^{-11}$	$(-5.84 \pm 0.26) \times 10^{-14}$	$(-2.05 \pm 0.02) \times 10^{-19}$
n-Dose 2 Scan 2	$(-4.54 \pm 0.02) \times 10^{-12}$	$(-1.66 \pm 0.03) \times 10^{-13}$	$(-1.95 \pm 0.06) \times 10^{-11}$	$(-5.71 \pm 0.33) \times 10^{-14}$	$(-2.39 \pm 0.02) \times 10^{-19}$
n-Dose 2 Scan 3	$(-5.01 \pm 0.02) \times 10^{-12}$	$(-1.74 \pm 0.04) \times 10^{-13}$	$(-1.99 \pm 0.05) \times 10^{-11}$	$(-5.77 \pm 0.27) \times 10^{-14}$	$(-3.13 \pm 0.02) \times 10^{-19}$

4. Discussion

Irradiated S2000, I302, sapphire, NBK7, and BK7G18 all exhibit negative NLA at 532 nm for nanosecond pulse duration, which could be attributed to the simultaneous effects of ultrafast TPA nonlinearity and the slow SA nonlinearity. These negative nonlinearities accompany radiation-induced linear attenuation, which we observed in the recent experiments with gamma- and neutron-irradiated glasses and sapphire [47]. In Figure 8 the ratio of the peak nonlinear transmission to the linear transmission for the irradiated samples is presented to illustrate how the negative NLA acts to compensate for some of the radiation-induced linear absorption [47].

S2000 and I302 each have trace elements of aluminium at $\leq$ 10 ppb and $\approx$ 20 ppm, respectively. Al-oxygen-hole-centers generated by gamma irradiation have been shown to cause a wide absorption band centered at 537 nm (FWHM 152 nm), which may be responsible for the radiation-induced linear absorption in S2000 and I302, and may also result in the SA effect resulting in negative nonlinear absorption [18, 20]. The difference in the magnitude of the NLA between S2000 and I302 may be associated with the significantly greater concentration of aluminum in I302. The reason that I302 requires a higher temperature of 600 °C to anneal, and that it retains a negative NLA coefficient during concurrent-irradiation thermal annealing, compared to S200, may be its low-OH content [48]. The low-OH content of I302 may result in an inability to passivate E' centers through the OH reaction with displaced oxygen and migration of the resultant interstitial water, and instead annealing the E' centers in I302 may be dependent on electron and hole excitation [48, 25].

The negative NLA observed in sapphire may be attributed to SA of a gamma-radiation induced composite V center defect [49, 28]. The composite V center produces a broad absorption band centered at 413 nm [28] that extends to the 532-nm wavelength of interest. The V centers are shown to anneal via thermal charge recombination.

NBK7 is a lead and arsenic-free version of BK7 borosilicate glass. NBK7 sensitivity to radiation-induced attenuation and darkening is well known, and thus it is not surprising that with significant radiation-induced attenuation, NBK7 also exhibits the greatest NLA effect in all of the samples measurement [26]. It is worthwhile to compare the nonlinear response of NBK7 to BK7G18. BK7G18 is doped with cerium at 1.8 w% to achieve radiation resistance. The cerium may be responsible for the significantly reduced negative nonlinearity compared to the NBK7 measurement, but it is also notable that *in-situ* measurements of irradiated BK7G18 have revealed that radiation-induced attenuation in BK7G18 exceeds that of NBK7 during irradiation [26]. The cerium doping does not negate the radiation damage in BK7G18 but makes the damage more thermally unstable and assists the annealing process so that it is possible BK7G18 may exhibit a significant NLA effect when under irradiation. Finally, the observable NLR in BK7G18 may be promoted by cerium doping as that is the most significant difference from NBK7 which had an uninterpreted NLR Z-scan similar to the other samples.

5. Conclusion

We have demonstrated the occurrence of negative nonlinear absorption in high-OH and low-OH content fused silica, sapphire, and two types of borosilicate glass when exposed to

ionizing radiation. The negative nonlinear absorption occurs as a result of both gamma and neutron radiation-induced defects, which expands on our previous results with Infrasil 302, and that radiation can also induce a negative NLR in BK7G18 [43]. The NLA effect is approximately proportional to the radiation-induced attenuation in each material as measured post-irradiation and contributes to mitigating absorption losses in the material for high-intensity laser pulses, which can be seen in Figure 8 [47]. Photobleaching has also been observed within low-OH content I302, NBK7, and BK7G18. Photobleaching makes a minor contribution to the observed negative nonlinearity, evident by the fact that all the Z-scan curves restore back to unity transmission after the sample transits the point of maximum intensity (position 0 mm). The photobleaching may provide a small annealing-like effect induced by the high-intensity laser pulse that, in conjunction with SA, reduces the radiation-induced attenuation losses.

This research explored the knowledge gap of radiation and thermal effects on nonlinear optical properties to inform the development of novel optical spectroscopic sensors for advanced fission reactors. An attractive direction for future work will be the use of shorter-pulse (picosecond to femtosecond) lasers to disambiguate the contribution of irradiation to slow and fast nonlinearities, which jointly comprise the nonlinear response measured with nanosecond Z-scan in this work.

6. Acknowledgments

This work has been supported by the U.S. Department of Energy, Nuclear Science User Facilities Program under award DE-NE0008906 and by the U.S. Department of Defense, Defense Threat Reduction Agency (HDTRA1-20-2-0002). B. W. M. has been supported by the U.S. Army Advanced Civil Schooling Program.

Data Availability

The data that support the findings of this study are available from the corresponding author upon reasonable request.

References

[1] M. Burger, L. Garrett, A. J. Burak, V. Petrov, A. Manera, P. Sabharwall, X. Sun, I. Jovanovic, Trace xenon detection in helium environment via laser-induced breakdown spectroscopy, Journal of Analytical Atomic Spectrometry 36 (2021) 824–828.

[2] J. F. Latkowski, A. Kubota, M. J. Caturla, S. N. Dixit, J. A. Speth, S. A. Payne, Fused silica final optics for inertial fusion energy: radiation studies and system-level analysis, Fusion Science and Technology 43 (4) (2003) 540–558.

[3] E. Colby, G. Lum, T. Plettner, J. Spencer, Gamma radiation studies on optical materials, IEEE Transactions on Nuclear Science 49 (6) (2002) 2857–2867.

[4] C. D. Orth, Vista – A vehicle for interplanetary space transport application powered by inertial confinement fusion, Tech. rep., Lawrence Livermore National Laboratory (03 2005).

[5] D. A. Cremers, L. J. Radziemski, Handbook of Laser-Induced Breakdown Spectroscopy, John Wiley & Sons, Ltd., West Sussex, UK, 2013.

[6] A. Williams, S. Phongikaroon, Laser-induced breakdown spectroscopy (libs) measurement of uranium in molten salt, Applied Spectroscopy 72 (7) (2018) 1029–1039.

[7] H. B. Andrews, J. McFarlane, Quantification of lanthanides in a molten salt reactor surrogate off-gas stream using laser-induced breakdown spectroscopy, Applied Spectroscopy 76 (2022) 877–886.

[8] H. B. Andrews, J. McFarlane, K. G. Myhre, Monitoring noble gases (Xe and Kr) and aerosols (Cs and Rb) in a molten salt reactor surrogate off-gas stream using laser-induced breakdown spectroscopy (LIBS), Applied Spectroscopy 76 (2022) 988–997.

[9] C. Li, C.-L. Feng, H. Y. Oderji, G.-N. Luo, H.-B. Ding, Review of libs application in nuclear fusion technology, Frontiers of Physics 11 (6) (2016). doi:10.1007/s11467-016-0606-1.

[10] G. S. Maurya, A. Marín-Roldán, P. Veis, A. K. Pathak, P. Sen, A review of the libs analysis for the plasma-facing components diagnostics, Journal of Nuclear Materials 541 (2020) 152417. doi:https://doi.org/10.1016/j.jnucmat.2020.152417.

[11] L. L. Chase, E. W. V. Stryland, Handbook of Laser Science and Technology Supplement 2: Optical Materials, 5th Edition, Vol. 2, CRC Press, New York, 1995, pp. 269–366.

[12] R. Kitamura, L. Pilon, M. Jonasz, Optical constants of silica glass from extreme ultraviolet to far infrared at near room temperature, Applied Optics 46 (33) (2007) 8118–8133.

[13] P. W. Levy, Color centers and radiation-induced defects in Al_2O_3, Physical Review 123 (4) (1961) 1226.

[14] W. Primak, E. Edwards, Radiation-induced dilatations in vitreous silica, Physical Review 128 (1962) 2580–2588.

[15] W. Primak, J. Luthra, Radiation induced expansion and increase in refractive index of magnesium oxide; evidence for the F center, Physical Review 150 (1966) 551–561.

[16] W. Primak, R. Kampwirth, The radiation compaction of vitreous silica, Journal of Applied Physics 39 (12) (1968) 5651–5658.

[17] G. J. Pogatshnik, Y. Chen, B. D. Evans, A model of lattice defects in sapphire, IEEE Transactions on Nuclear Science 34 (6) (1987) 1709–1712.

[18] H. Hosono, H. Kawazoe, Radiation-induced coloring and paramagnetic centers in synthetic siO_2:Al glasses, Nuclear Instruments and Methods in Physics Research Section B: Beam Interactions with Materials and Atoms 91 (1) (1994) 395–399.

[19] G. P. Pells, Radiation damage effects in alumina, Journal of the American Ceramic Society 77 (2) (1994) 368–377.

[20] C. D. Marshall, J. A. Speth, S. A. Payne, Induced optical absorption in gamma, neutron and ultraviolet irradiated fused quartz and silica, Journal of Non-Crystalline Solids 212 (1997) 59–73.

[21] A. Islamov, E. Ibragimova, I. Nuritdinov, Radiation-optical characteristics of quartz glass and sapphire, Journal of Nuclear Materials 362 (2007) 222–226.

[22] G. Sharma, K. S. Thind, H. Singh, L. Gerward, Optical properties of heavy metal oxide glasses before and after γ-irradiation, Physica Status Solidi A 204 (2) (2007) 591–601.

[23] A. K. Sandhu, S. Singh, O. P. Pandey, Gamma ray induced modifications of quaternary silicate glasses, Journal of Physics D: Applied Physics 41 (16) (2008) 165402.

[24] A. K. Sandhu, S. Singh, O. P. Pandey, Neutron irradiation effects on optical and structural properties of silicate glasses, Materials Chemistry and Physics 115 (2) (2009) 783–788.

[25] P. Martín, M. León, A. Ibarra, E. R. Hodgson, Thermal stability of gamma irradiation induced defects for different fused silica, Journal of Nuclear Materials 417 (1-3) (2011) 818–821.

[26] S. Girard, T. Allanche, P. Paillet, V. Goiffon, M. V. Uffelen, L. Mont-Casellas, C. Muller, A. Boukenter, Y. Ouerdane, W. D. Cock, Growth and decay kinetics of radiation-induced attenuation in bulk optical materials, IEEE Transactions on Nuclear Science 65 (8) (2017) 1612–1618.

[27] C. M. Petrie, B. Wilson, T. E. Blue, In situ gamma radiation-induced attenuation in sapphire optical fibers heated to 1000 °C, Journal of the American Ceramic Society 97 (10) (2014) 3150–3156.

[28] C. M. Petrie, W. Windl, T. E. Blue, In-situ reactor radiation-induced attenuation in sapphire optical fibers, Journal of the American Ceramic Society 97 (12) (2014) 3883–3889.

[29] C. M. Petrie, T. E. Blue, In situ reactor radiation-induced attenuation in sapphire optical fibers heated up to 1000 °C, Nuclear Instruments and Methods in Physics Research B 342 (2015) 91–97.

[30] C. M. Petrie, A. Birri, T. E. Blue, High-dose temperature-dependent neutron irradiation effects on the optical transmission and dimensional stability of amorphous fused silica, Journal of Non-Crystalline Solids 525 (2019) 119668.

[31] C. M. Petrie, A. Birri, T. E. Blue, Optical transmission and dimensional stability of single-crystal sapphire after high-dose neutron irradiation at various temperatures up to 688 °C, Journal of Nuclear Materials 559 (2022) 153432.

[32] M. Sheik-bahae, A. A. Said, E. V. Stryland, High-sensitivity, single-beam n_2 measurements, Optics Letters 14 (17) (1989) 955–957.

[33] D. J. Musgraves, J. Hu, L. Calvez (Eds.), Springer Handbook of Glass, Springer International Publishing, Gewerbestrasse 11, 6330 Cham, Switzerland, 2019, pp. 169–191. doi:10.1007/978-3-319-93728-1.

[34] E. V. Stryland, M. Shiek-Bahae, Z-Scan Measurements of Optical Nonlinearities, Marcel Dekker, Inc., New York, 1998.

[35] T. Olivier, F. Billard, H. Akhouayri, Z-scan theoretical and experimental studies for accurate measurements of the nonlinear refractive index and absorption of optical glasses near damage threshold, Proceedings SPIE 5273 (2004) 341–349.

[36] J. Wang, B. Gu, H.-T. Wang, X.-W. Ni, Z-scan analytical theory for material with saturable absorption and two-photon absorption, Optics Communications 283 (18) (2010) 3525–2528.

[37] F. Billard, T. Olivier, H. Akhouayri, Study and experimental setting of the z-scan method for accurate nonlinear refractive index and absorption metrology, Proceedings SPIE 5273 (2004).

[38] Y.-L. Huang, C.-K. Sun, J.-C. Liang, S. Keller, M. P. Mack, U. K. Mishra, S. P. DenBaars, Femtosecond z-scan measurement of GaN, Applied Physics Letters 75 (22) (1999) 3524–3526.

[39] T. Miyoshi, N. Matsuo, P. Maly, F. Trojanek, P. Nemec, J. Kudrna, Negative and positive nonlinear absorption in CdS-doped glasses, Journal of Materials Science Letters 20 (2001) 343–345.

[40] A. Scalisi, G. Compagnini, L. D'Urso, O. Puglisi, Nonlinear optical activity in Ag–SiO_2 nanocomposite thin films with different silver concentration, Applied Surface Science 226 (1) (2004) 237–241.

[41] J. Olesiak-Banska, M. Waszkielewicz, K. Matczyszyn, M. Samoc, A closer look at two-photon absorption, absorption saturation and nonlinear refraction in gold nanoclusters, RSC Advances 6 (2016) 98748–98752.

[42] V. Sreeja, A. Cheruvalathu, R. Reshmi, E. Anila, S. Thomas, M. Jayaraj, Effect of thickness on nonlinear absorption properties of graphite oxide thin films, Optical Materials 60 (2016) 450–455.

[43] B. W. Morgan, M. P. V. Zile, P. Sabharwall, M. Burger, I. Jovanovic, Gamma-radiation-induced negative nonlinear absorption in quartz glass, Optical Materials Express 12 (2022) 1188–1197.

[44] B. W. Morgan, M. V. Zile, P. Sabharwall, M. Burger, I. Jovanovic, Post-irradiation examination of optical components for advanced fission reactor instrumentation, Review of Scientific Instruments 90 (10) (2021) 105107.

[45] P. B. Chapple, J. Staromlynska, J. A. Hermann, T. J. McKay, Single-beam z-scan: Measurement techniques and analysis, Journal of Nonlinear Optical Physics and Materials 6 (3) (1997) 251–293.

[46] S. White, Neutron Spectrum Measurement within the 6.5-inch Tube Furnace, Tech. rep., The Ohio State University (09 2021).

[47] B. W. Morgan, M. P. V. Zile, C. M. Petrie, P. Sabharwall, M. Burger, I. Jovanovic, Optical absorption of fused silica and sapphire exposed to neutron and gamma radiation with simultaneous thermal annealing, Journal of Nuclear Materials 570 (2022) 153945.

[48] D. L. Griscom, Characterization of three E'-center variants in X- and γ-irradiated high purity α-SiO_2, Nuclear Instruments and Methods in Physics Research Section B: Beam Interactions with Materials and Atoms 1 (2) (1984) 481–488.

[49] T. J. Turner, J. H. Crawford, V centers in single crystal Al_2O_3, Solid State Communications 17 (2) (1975) 167–169.

Appendix A. Photobleaching Z-scans

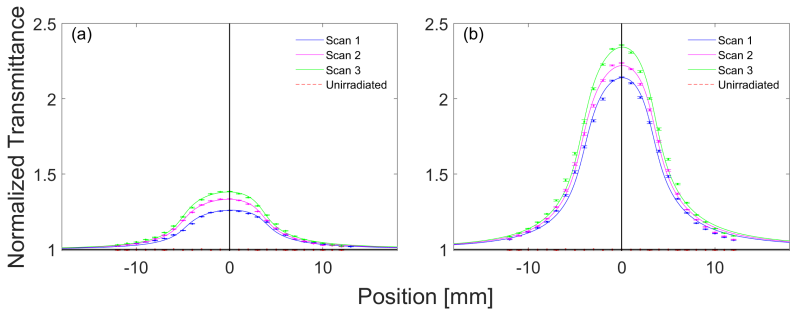

Figure A.9: Three consecutive NLA Z-scans of I302 at the same location in the sample after irradiation to (a) n-Dose 1 and (b) n-Dose 2, performed to test the photobleaching effect. NLA coefficient values are provided in Table 4.

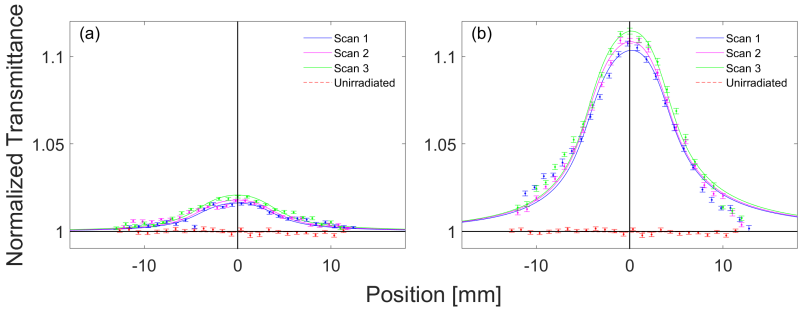

Figure A.10: Three consecutive NLA Z-scans of sapphire at the same location in the sample after irradiation to (a) n-Dose 1 and (b) n-Dose 2, performed to test the photobleaching effect. NLA coefficient values are provided in Table 4.

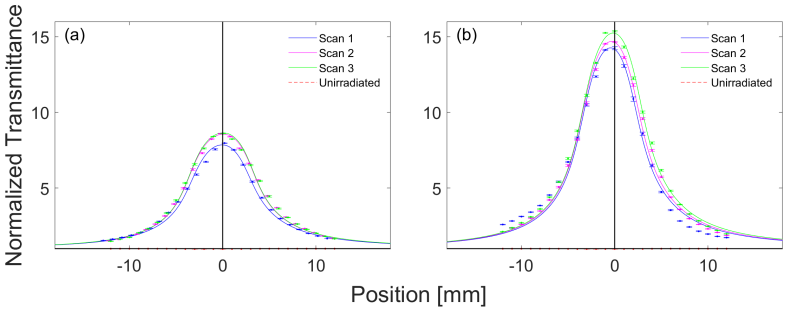

Figure A.11: Three consecutive NLA Z-scans of NBK7 at the same location in the sample after irradiation to (a) n-Dose 1 and (b) n-Dose 2, performed to test the photobleaching effect. NLA coefficient values are provided in Table 4.

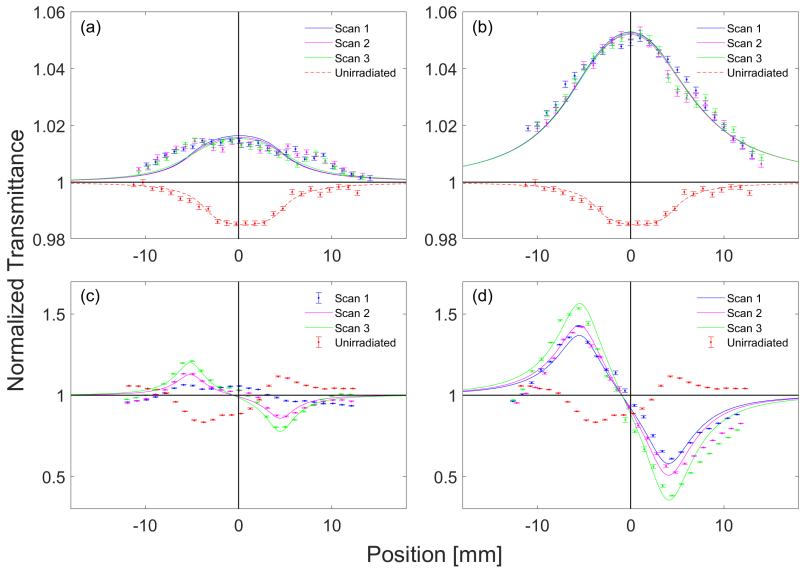

Figure A.12: Three consecutive NLA Z-scans of BK7G18 at the same location in the sample after irradiation to (a) n-Dose 1 and (b) n-Dose 2, performed to test the photobleaching effect. The corresponding three NLR Z-scans are provided in (c) and (d). Z-scans in (c) and (d) without a fit line were unable to be reliably simulated. NLA and NLR coefficient values are provided in Table 4.